# Nanogap-Resolved Adsorption-Coupled Electron Transfer by Scanning Electrochemical Microscopy: Implications for Electrocatalysis

Niraja Kurapati,<sup>†</sup> Donald C. Janda,<sup>†</sup> Ryan J. Balla,<sup>†</sup> Siao-Han Huang,<sup>†</sup> Kevin C. Leonard,<sup>‡</sup> and Shigeru Amemiya,<sup>†</sup>,\*

- <sup>†</sup> Department of Chemistry, University of Pittsburgh, 219 Parkman Avenue, Pittsburgh, Pennsylvania, 15260, United States
- ‡ Center for Environmentally Beneficial Catalysis, Department of Chemical and Petroleum Engineering, University of Kansas, 1501 Wakarusa Drive, Lawrence, Kansas 66047, United States

ABSTRACT: Herein, we demonstrate for the first time that the mechanism of adsorption-coupled electron-transfer (ACET) reactions can be identified experimentally. The electron transfer (ET) and specific adsorption of redox-active molecules are coupled in many electrode reactions with practical importance and fundamental interest. ACET reactions are often represented by the concerted mechanism. In reductive adsorption, an oxidant is simultaneously reduced and adsorbed as a reductant on the electrode surface through the ACET step. Alternatively, the non-concerted mechanism mediates outer-sphere reduction and adsorption separately when the reductant adsorption is reversible. In electrocatalysis, reversibly adsorbed reductants are ubiquitous and crucial intermediates. Moreover, electrocatalysis is complicated by the mixed mechanism based on simultaneous ACET and outer-sphere ET steps. In ths work, we reveal the non-concerted mechanism for ferrocene derivatives adsorbed at highly oriented pyrolytic graphite as simple models. We enable the transient voltammetric mode of nanoscale scanning electrochemical microscopy (SECM) to kinetically control the adsorption step, which is required for the discrimination of non-concerted, concerted, and mixed mechanisms. Experimental voltammograms are compared with each mechanism by employing the finite element simulation. The non-concerted mechanism is supported to indicate that the ACET step is intrinsically slower than the outer-sphere counterpart by at least four orders of magnitude. This finding implies that an ACET step is facilitated thermodynamically but may not be necessarily accelerated or catalyzed by the adsorption of the reductant. Significantly, SECM-based transient voltammetry will become a powerful tool to resolve and understand electrocatalytic ACET reactions at the elementary level.

The coupling between electron transfer (ET) and specific adsorption of redox-active molecules at the electrode surface is imperative in both applied and fundamental electrochemistry. The adsorption-coupled electron-transfer (ACET) reactions are often considered to proceed in a single step, e.g., reductive adsorption. In this concerted mechanism, Andrew and Adsorption (9 (= H<sup>+</sup>, Li<sup>+</sup>, O<sub>2</sub>, CO<sub>2</sub>, etc.), is simultaneously reduced and adsorbed through the ACET step to deposit a reductant, R<sub>ads</sub>, on the electrode surface

$$O + e \blacksquare R_{ads}$$
 (1)

The adsorbate serves as a crucial intermediate or a product in many electrode reactions with great importance and interest as exemplified by electrocatalysis, <sup>1,5,6</sup> electrodeposition, <sup>7</sup> and electrointercalation. <sup>8</sup> Alternatively, an ACET reaction may proceed through the non-concerted mechanism based on separate ET and adsorption steps, <sup>2,4</sup> i.e., reduction and adsorption, respectively. Practically, both ACET and non-ACET steps may occur simultaneously in the mixed mechanism.

Recently, we demonstrated that concerted and nonconcerted mechanisms of ACET reactions have not been discriminated experimentally.4 The two mechanisms were proposed five decades ago9 but systematically compared only recently.2,4 Theoretically, unique voltammograms are expected for each mechanism to discriminate between the two mechanisms if the adsorption step is kinetically controlled<sup>2,4</sup> and the ET steps are chemically reversible.<sup>4</sup> Only one of the two requirements, however, has been met experimentally10 to yield identical voltammograms for both mechanisms.4 Problematically, experimental voltammograms of ACET reactions have been assessed by considering only the concerted11 or non-concerted10,12 mechanism, thereby preventing the unambiguous determination of the reaction mechanism.4 Moreover, the mixed mechanism has been considered theoretically by assuming the arbitrary sequence of ACET and non-ACET steps not the simultaneous occurrence of the two ET steps.13

Our current understanding of electrocatalysis is limited by the ambiguity in the mechanism of ACET reactions.<sup>2,4</sup>

In many electrocatalytic reactions, a reductant is reversibly adsorbed

$$R \blacksquare R_{ads}$$
 (2)

to enable not only ACET (eq 1) but also outer-sphere ET

$$O + e \blacksquare R \tag{3}$$

For instance, both adsorbed and non-adsorbed forms of  $O_2$ - were detected experimentally<sup>14,15</sup> for the one-electron reduction of  $O_2$ , which controls the rate and product of the entire oxygen reduction reaction.<sup>16,17</sup> Similarly, the overall  $CO_2$  reduction reaction is controlled by the one-electron  $CO_2$  reduction,<sup>18,19</sup> which yields both adsorbed and non-adsorbed forms of  $CO_2$ - as observed experimentally.<sup>20,21</sup> It, however, has not been determined experimentally whether a reductant,  $R_{ads}$  or R, is produced from an oxidant, O, through an ET step or ET and adsorption steps. Moreover, electrocatalytic ACET reactions are complicated by coupling with multiple ET, adsorption, and desorption steps as well as homogeneous and surface chemical steps.<sup>12,22</sup> Irreversible chemical steps<sup>10,23</sup> prevent the determination of the ACET mechanism.<sup>4</sup>

Herein, we report for the first time that the mechanism of ACET reactions can be determined experimentally. We nanoscale scanning electrochemical microscopy<sup>24,25</sup> (SECM) to confirm the non-concerted mechanism of ferrocene derivatives at highly oriented pyrolytic graphite (HOPG) as simple models. Previously, we employed cyclic voltammetry (CV) to demonstrate quantitatively that only the reduced form of the ferrocene derivatives is adsorbed on HOPG (eq 2).26,27 The experimental CVs, however, agreed with both non-concerted (eq 3) and concerted (eq 1) mechanisms because all steps were diffusion-controlled to maintain the thermodynamic equivalence between the two mechanisms.4 In this work, we develop the transient voltammetric mode of nanoscale SECM to kinetically control the common adsorption step as required for the identification of the ACET mechanism.<sup>2,4</sup> This unprecedented achievement is made by increasing the scan rate up to 10 V/s from 0.05 V/s in our previous studies.<sup>28,29</sup> We find that the ACET step is intrinsically slower than the outer-sphere counterpart at least by four orders of magnitude to manifest the nonconcerted mechanism neither concerted nor mixed mechanism.

#### **EXPERIMENTAL SECTION**

The redox reactions of (ferrocenylmethyl)trimethylammonium (FcTMA+) and ferroceneacetate (FcCH2COO-) at HOPG were investigated by employing nanoscale SECM as detailed in SI. HOPG (SPI-1 grade, SPI, West Chester, PA) was peeled in the filtered air as humidified over dry ice to minimize the airborne contamination of the exposed surface.<sup>29,30</sup> Freshly peeled HOPG was immediately set up in the SECM cell that was sealed to prevent the airborne contamination of the solution (Figure S-1). The ferrocene solution was prepared from ultrapure water with a resistivity of 18.2 M $\Omega$  cm and a total organic carbon of 2-3 ppb.

The transient voltammetric mode of nanoscale SECM was enabled by using two potentiostats (Figure S-1) to quantitatively investigate adsorption effects. The potential of HOPG was cycled at up to 10 V/s with the electronic compensation of ohmic potential drop owing to the mA current by using a potentiostat (CHI 660B, CH Instruments, Austin, TX). The three-electrode cell was equipped with a Pt counter electrode and a Pt quasi-reference electrode. The potentiostat was floating<sup>31</sup> and isolated from a grounded patch-clamp amplifier (Axopatch 200B, Molecular Devices, San Jose, CA) as the second potentiostat for the measurement of the low-nA tip current with 0.1 ms resolution. The amplifier recorded the amperometric current of a Pt tip at a fixed potential in a two-electrode cell with a Pt quasi-reference/counter electrode. The cycle of the substrate potential was synchronized with the measurement of the tip current by using a digital switch with an optical coupler,32 which isolated the floating potentiostat from the grounded amplifier.

A sharp, flat, and damage-free tip was positioned at a distance, *d*, of ~50 nm from the atomically flat HOPG surface as established previously. <sup>28,29</sup> Specifically, an ~1 µm-diameter Pt tip was surrounded by a thin glass sheath with an outer diameter of ~2 µm and flattened by focused-ion-beam milling (Figure S-2A). <sup>33,34</sup> The tip was protected from electrostatic damage <sup>35-37</sup> as confirmed after SECM experiments (Figure S-2B). The tip–HOPG distance was controlled precisely and quickly by measuring an approach curve in the intelligent mode <sup>37,38</sup> to prevent the tip–substrate contact (Figure S-3) and minimize the fouling of the HOPG surface by residual contaminants in redox molecules, <sup>28</sup> respectively. The tip–substrate nanogap was maintained by minimizing the thermal drift of the tip by using a homebuilt isothermal chamber. <sup>39</sup>

The amperometric tip current,  $i_T$ , was free from the capacitive current and directly compared with the tip current simulated for non-concerted, concerted, and mixed mechanisms as detailed in SI. Only the rate constant of ferrocene desorption from HOPG,  $k_{\rm des}$ , was adjusted. Other parameters were determined by CV.<sup>26,27</sup> Experimental and simulated voltammograms were compared by normalizing the tip current against the diffusion-limited tip current,  $i_{\rm T,\infty}$ , in the bulk solution<sup>40</sup>

$$i_{T,\infty} = 4\beta nDFc_0 a \tag{4}$$

where the current due to oxidation has a positive sign,<sup>41</sup>  $\beta$  is a function of RG (=  $r_{\rm g}/a$  =~2;  $r_{\rm g}$  and a are outer and inner tip radii, respectively), n is the number of the transferred electrons, and D and  $c_{\rm o}$  are the diffusion coefficient and concentration of the ferrocene derivatives in the solution.

#### **RESULTS AND DISCUSSION**

Non-Concerted Oxidation and Desorption of FcT-MA<sup>+</sup>. We developed the transient voltammetric mode of nanoscale SECM to identify the non-concerted oxidation and desorption of FcTMA<sup>+</sup>. FcTMA<sup>+</sup> was present in the solution and adsorbed on HOPG to yield an initial coverage of 0.51<sup>26</sup> from the isotherm (eq S-3). FcTMA<sup>+</sup> was oxi-

dized voltammetrically at HOPG to amperometrically detect the substrate-generated ferrocenium, Fc+TMA+, by the tip positioned at ~50 nm from HOPG. In the non-concerted mechanism (Figure 1A), the non-adsorbed form of FcTMA+ was oxidized through the outer-sphere ET step, where the adsorbate was desorbed and oxidized. In the concerted mechanism (Figure 1B), the adsorbate was

oxidized through the ACET step, where the non-adsorbed form of FcTMA+ was adsorbed and oxidized. In the mixed mechanism (Figure 1C), the adsorbate was desorbed and oxidized through the outer-sphere step or oxidized through the ACET step. Both forward and reverse directions of adsorption and ET steps were considered in the simulation of each mechanism.

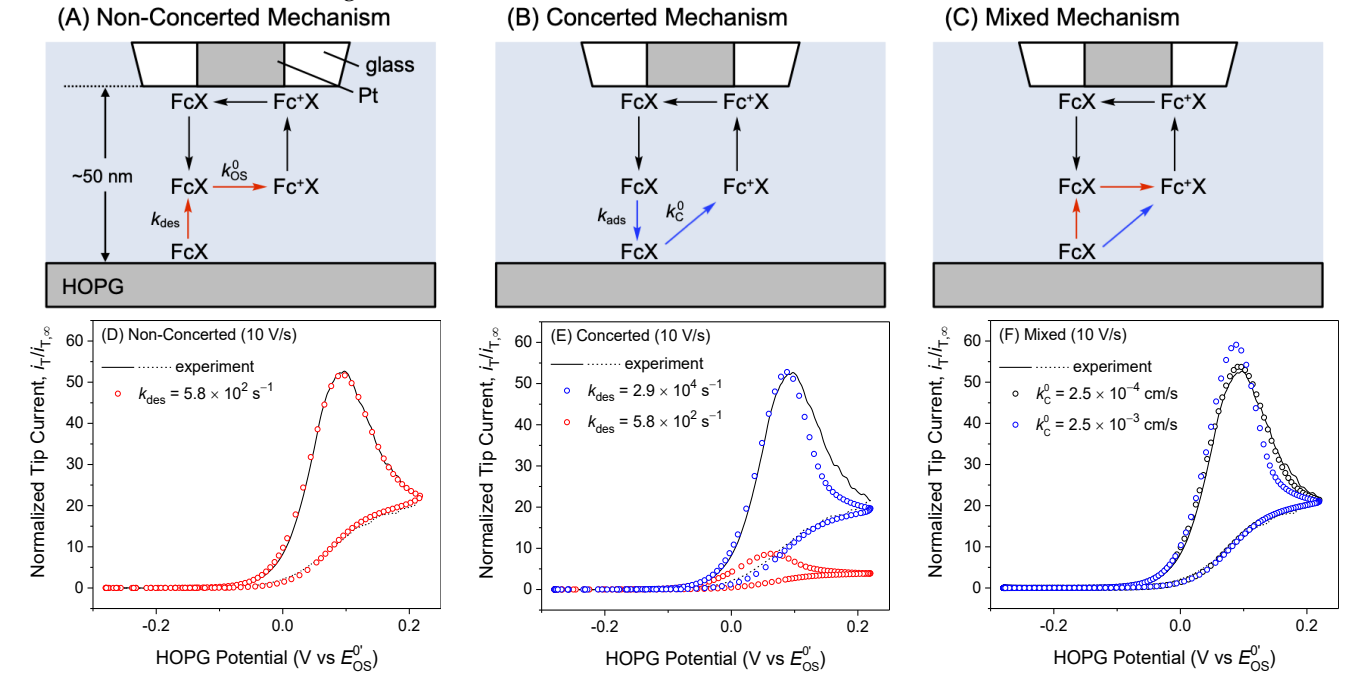


**Figure 1.** Scheme of SECM measurement of FcTMA+ oxidation at HOPG through (A) non-concerted, (B) concerted, and (C) mixed mechanisms. FcX and FcX+ represent ferrocene and ferrocenium, respectively. (D), (E), and (F) The finite element analysis of the identical experimental tip current versus the cycled HOPG potential at 10 V/s with different mechanisms. The experimental curve was obtained with 0.3 mM FcTMAPF<sub>6</sub> in 1 M KCl for  $i_{T,\infty}$  = 32 pA during forward anodic and reverse cathodic scans (solid and dotted lines, respectively). Simulated curves (circles) were obtained with a = 560 nm, RG = 1.8, and d = 48 nm. ET steps were electrochemically reversible except for the ACET step in part F, where  $k_{\text{des}}$  = 5.8 × 10<sup>2</sup> s<sup>-1</sup>.

We employed the fast scan rate of 10 V/s to find that the plot of the tip current versus the HOPG potential agreed with the simulation of the non-concerted mechanism (lines and circles, respectively, in Figure 1D). The tip current was enhanced to peak at  $i_T/i_{T,\infty} = 53$  during the forward anodic scan, where Fc+TMA+ was generated from both adsorbed and non-adsorbed forms of FcTMA+ at HOPG. The best fit between experimental and simulated voltammograms yielded  $k_{\rm des} = 5.8 \times 10^2 \, \rm s^{-1}$  for ferrocene desorption from HOPG. A standard rate constant of ≥17 cm/s was employed to represent the electrochemically reversible outer-sphere ET step. The minimum high as estimated previously at 0.05 V/s and as predicted by the Marcus theory. 28,29 The experimental voltammograms were highly reproducible to yield average  $k_{\text{des}}$  of  $(6.6 \pm 0.7) \times 10^2 \text{ s}^{-1} (N = 9)$ . The highly precise determination of  $k_{des}$  is attributed also to the high sensitivity of the tip current to  $k_{\text{des}}$  (Figure S-5A).

By contrast, we were not able to fit experimental voltammograms with the voltammograms simulated for the concerted mechanism (lines and blue circles, respectively, in Figure 1E). The concerted mechanism yielded a narrower peak with a width of 0.12 V at half height than the

experimental width of 0.14 V. The narrower width is determined by the potential dependence of the electrochemically reversible ACET step with a standard rate constant of ≥ 0.25 cm/s. The broader peak of the nonconcerted mechanism represents that the potential-independent desorption of FcTMA+ can be delayed from the potential scan.4 This result confirms that nonconcerted and concerted mechanisms can be discriminated against each other when the common adsorption step is kinetically controlled.4 The two mechanisms coupled with the equilibrium adsorption step yield the identical voltammogram (Figure S-6A).

Moreover, the concerted mechanism required erroneously high  $k_{\rm des}$  of 2.9 × 10<sup>4</sup> s<sup>-1</sup> to match the experimental peak current with the simulated peak current (Figure 1E). High  $k_{\rm des}$  corresponds to a high adsorption rate constant,  $k_{\rm ads}$ , because their ratio was fixed by an equilibrium constant,  $\beta_{\rm R}$  (=  $k_{\rm ads}/k_{\rm des}$ ), in our simulation. A very low tip current was simulated for the concerted mechanism with  $k_{\rm des} = 5.8 \times 10^2 \, {\rm s}^{-1}$  (red circles), which was determined for the non-concerted mechanism (Figure 1D). In the concerted mechanism, the adsorption of FcTMA<sup>+</sup> must be fast to sustain the adsorption-coupled oxidation of FcT- MA<sup>+</sup> and, subsequently, enhance the tip current (Figure 1B). By contrast, the outer-sphere oxidation step of the non-concerted mechanism can be sustained by regenerating FcTMA<sup>+</sup> at the tip to enhance the tip current despite the slow desorption of FcTMA<sup>+</sup> (Figure 1A).

We also examined the mixed mechanism (Figure 1C) not only to obtain a poor fit with the experimental voltammogram but also to estimate. We employed the same parameters as determined for the outer-sphere ET and adsorption steps of the non-concerted mechanism and adjusted only. The experimental voltammogram fitted the voltammogram simulated with of up to 2.5 × 10<sup>-4</sup> cm/s (black circles in Figure 1F). Higher yielded a higher and narrower voltammetric peak (blue circles) than the experimental peak. The maximum of 2.5 × 10<sup>-4</sup> cm/s for a good fit is much lower than the minimum of 17 cm/s as determined for the non-concerted mechanism. This result indicates that the ACET step was at least 6.8 × 10<sup>4</sup> times intrinsically slower than the outer-sphere ET step and, subsequently, was not observed.

**Confirmation of Non-Concerted Oxidation Mechanism.** We further confirmed the non-concerted mechanism for FcTMA+ oxidation at HOPG. Experimentally, we confirmed the non-concerted mechanism at slower scan rates of 5, 3, 1, and 0.1 V/s (Figure S-7). At 5 V/s, the adsorption step was kinetically controlled to fit the experimental voltammogram with the non-concerted mechanism but not with the concerted mechanism. The two mechanisms yielded identical voltammograms at 3, 1, and 0.1 V/s, thereby indicating that the adsorption step became diffusion-controlled to prevent the identification of the ACET mechanism.  $^{2,4}$  We, however, excluded the concerted mechanism, which required erroneously high  $k_{\rm des}$  of  $>10^4$  s<sup>-1</sup> to fit experimental voltammograms at slow scan rates. By contrast, the experimental voltammograms fit-

ted well with the non-concerted mechanism with consistent  $k_{\text{des}}$  at all scan rates.

We also found that the implementation of additional steps into the concerted mechanism did not improve the fit with experimental voltammograms. We considered the lateral diffusion of FcTMA+ adsorbed on HOPG because the local concentration of the adsorbate under the tip was modulated by the tip reaction to generate a lateral concentration gradient.42 The simulated voltammogram, however, was not broadened and was lowered for both concerted and non-concerted mechanisms to deviate from the experimental voltammogram (Figure S-9). Moreover, we considered the adsorption of Fc+TMA+ on the glass sheath of a Pt tip,43 which only lowered the tip current for both mechanisms (Figure S-10). These results confirm that the surface diffusion of FcTMA+ and the glass adsorption of Fc+TMA+ had a negligible effect on the tip current. It should be noted that the adsorption of ferrocene derivatives on Pt was excluded experimentally<sup>26,27</sup> and is not relevant to this work because the tip reaction is diffusion-limited.

Non-Concerted Reduction and Adsorption of Fc+TMA+. We also investigated Fc+TMA+ reduction at HOPG by nanoscale SECM to confirm the non-concerted mechanism. In this experiment, Fc+TMA+ was generated from FcTMA+ amperometrically at the tip and reduced voltammetrically at HOPG with a separation of ~50 nm. In the non-concerted mechanism (Figure 2A), Fc+TMA+ was reduced through the outer-sphere ET step, where FcTMA+ was adsorbed or transported to the tip. In the concerted mechanism (Figure 2B), Fc+TMA+ was reduced to the adsorbate through the ACET step. The adsorbate must be desorbed from HOPG to react at the tip. In the mixed mechanism (Figure 2C), Fc+TMA+ was reduced competitively through ACET and outer-sphere ET steps. Both directions of adsorption and ET steps were considered in the simulation of each mechanism.

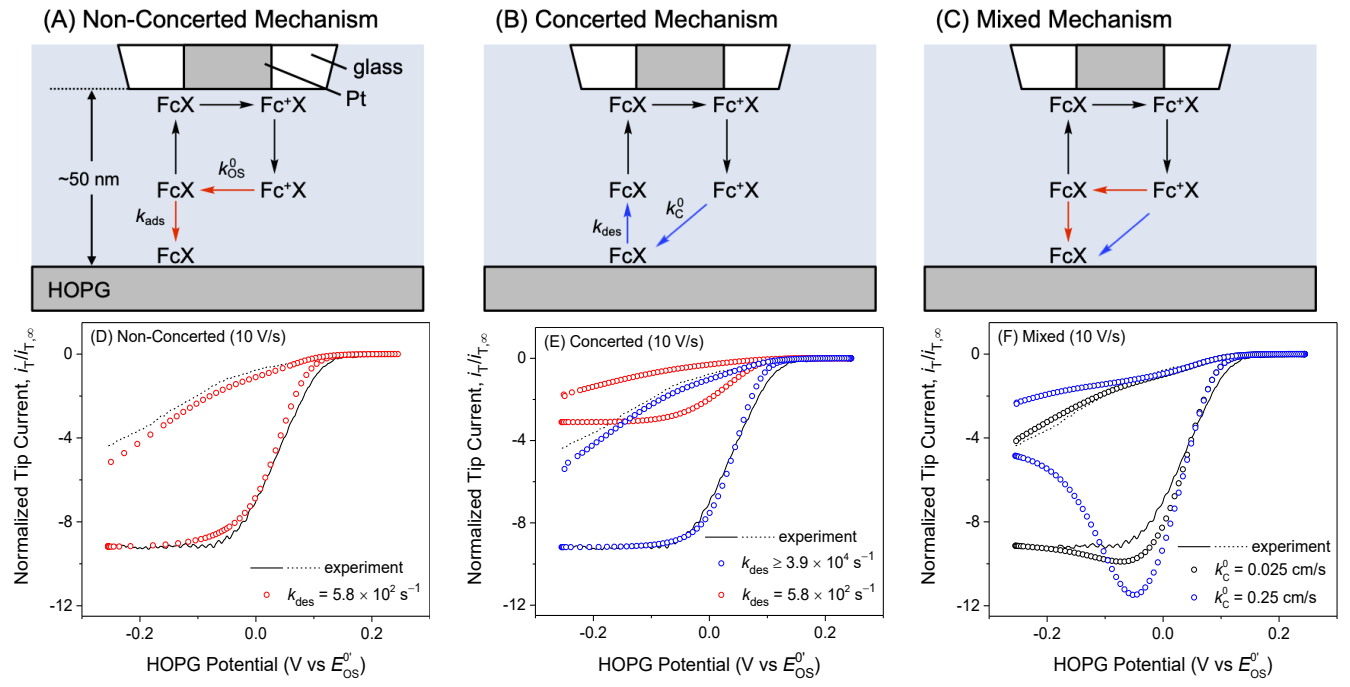


**Figure 2.** Scheme of SECM measurement of Fc<sup>+</sup>TMA<sup>+</sup> reduction at HOPG through (A) non-concerted, (B) concerted, and (C) mixed mechanisms. FcX and FcX<sup>+</sup> represent ferrocene and ferrocenium, respectively. (D), (E), and (F) The finite element analysis of the identical experimental tip current versus the HOPG potential at 10 V/s with different mechanisms. The experimental curve was obtained with 0.3 mM FcTMAPF<sub>6</sub> in 1 M KCl for  $i_{T,\infty} = 32$  pA during forward anodic and reverse cathodic scans (solid and dotted lines, respectively). Simulated curves (circles) were obtained with a = 560 nm, RG = 1.8, and d = 48 nm. ET steps were electrochemically reversible except for the ACET step in part F, where  $k_{\text{des}} = 5.8 \times 10^2 \text{ s}^{-1}$ .

Experimental voltammograms of Fc+TMA+ reduction at HOPG fitted well with the non-concreted mechanism (Figure 2D) by employing the same parameters as determined for the non-concerted FcTMA+ oxidation (Figure 1D). The simulated voltammogram employed  $k_{\rm des}$  of 5.8 × 10<sup>2</sup> s<sup>-1</sup> and an electrochemically reversible outer-sphere ET step. The experimental voltammogram also fitted well with the concerted mechanism but required extremely high  $k_{\rm des}$  of 2.9 × 10<sup>4</sup> s<sup>-1</sup> (blue circles in Figure 2E). The high  $k_{\text{des}}$  failed to fit the experimental voltammogram of FcTMA<sup>+</sup> oxidation (Figure 1E). The erroneously high  $k_{\text{des}}$  is needed to enhance the tip current in the concerted mechanism (Figure 2B). This is not the case for the nonconcerted mechanism (Figure 2A), where the nonadsorbed form of FcTMA+ was regenerated from Fc+TMA+ at HOPG to enhance the tip current. Similarly, experimental voltammograms at 0.1-5 V/s support the nonconcerted mechanism with consistent  $k_{des}$  and exclude the concerted mechanism, which requires erroneously high  $k_{\text{des}}$  (Figure S-8).

The experimental voltammogram did not fit with the mixed mechanism when the ACET step became significantly fast ( $\ge 2.5 \times 10^{-2} \text{ cm/s}$  in Figure 2F), thereby confirming the non-concerted mechanism. The minimum was erroneously high because it exceeded the maximum of  $2.5 \times 10^{-4} \text{ cm/s}$  that was required to obtain a good fit for FcTMA+ oxidation at HOPG (Figure 1F). Notably, the voltammograms simulated with  $\ge 2.5 \times 10^{-2} \text{ cm/s}$  showed a forward peak, which resulted from the accumulation of the adsorbate under the tip before the potential scan.

Effect of Adsorbate–Adsorbate Attractions. Since this work is the first to experimentally determine the ACET mechanism, we generalized our finding of the nonconcerted mechanism by investigating FcCH<sub>2</sub>COO<sup>-</sup> with adsorbate–adsorbate attractions on HOPG.<sup>27</sup> FcCH<sub>2</sub>COO<sup>-</sup> is anionic and readily dissolved in the solution at pH 6.2 but is attracted to each other on HOPG by presumably sharing co-adsorbed aqueous cations between carboxylate groups. The co-adsorption of aqueous cations maintains the electroneutrality of the double-layer region and accounts for the potential independence of the adsorption isotherm<sup>27</sup> (eq S-3), which yields an initial coverage of 0.35. The adsorbate–adsorbate interaction, , of +3.5<sup>27</sup> and -0.3<sup>26</sup> in the isotherm was determined for FcCH<sub>2</sub>COO<sup>-</sup> and FcTMA<sup>+</sup>, respectively, by CV.

Experimental voltammograms of FcCH<sub>2</sub>COO<sup>-</sup> oxidation at HOPG at 10 V/s agreed well with the non-concerted mechanism (lines and circles, respectively, in Figure 3A). The tip current peaked at  $i_{\rm T}/i_{\rm T,\infty}=78$  during the forward anodic scan to yield  $k_{\rm des}=4.7\times10^2~{\rm s}^{-1}$ . The outer-sphere ET step was electrochemically reversible as represented by  $\ge 13~{\rm cm/s}$ . The simulated voltammogram was highly sensitive to the desorption rate constant (Figure S-5C). Average  $k_{\rm des}$  of  $(4.9\pm0.3)\times10^2~{\rm s}^{-1}$  (N=8) was determined precisely from highly reproducible experimental voltammograms. FcCH<sub>2</sub>COO<sup>-</sup> and FcTMA<sup>+</sup> had similar  $k_{\rm des}$ . FcCH<sub>2</sub>COO<sup>-</sup>, however, yielded a narrower peak width of 0.11 V at half height owing to adsorbate–adsorbate attractions.

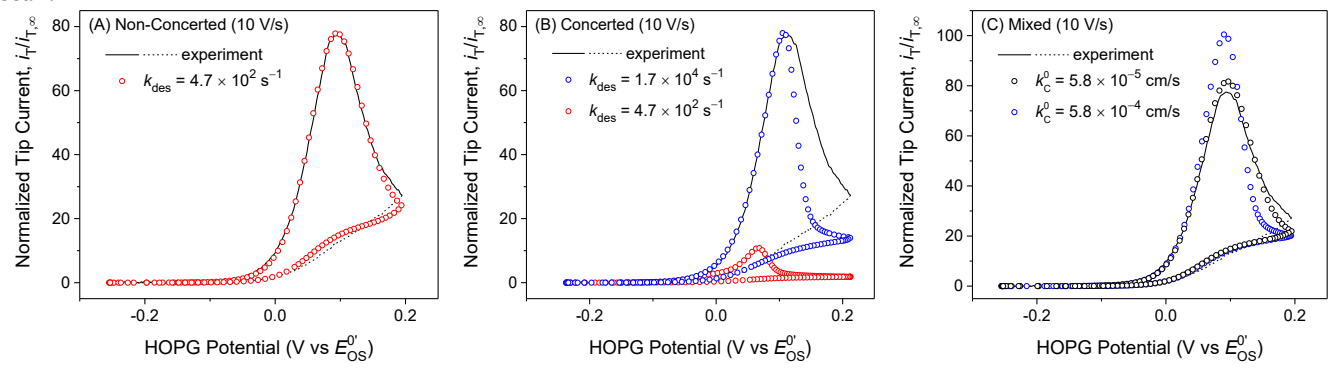


**Figure 3.** SECM measurement of FcCH₂COO⁻ oxidation at HOPG at 10 V/s as compared with (A) non-concerted, (B) concerted, and (C) mixed mechanisms. The identical experimental curve was obtained with 0.1 mM FcCH₂COOH in 1 M KCl and 0.1 M phosphate buffer (pH = 6.2) for  $i_{T,\infty}$  = 7.1 pA during forward anodic and reverse cathodic scans of the HOPG potential (solid and dotted lines, respectively). Simulated curves (circles) were obtained with a = 333 nm, RG = 2.3, and d = 30 nm. The outer-sphere ET step was electrochemically reversible in parts (A) and (C). The ACET step was quasi-reversible in part B with a = 4.9 × 10⁻² cm/s and part C with as given in the figure and a a0 states a1.

The concerted mechanism was excluded because the simulated voltammetric peak was too narrow to fit the

experimental peak (blue circles and lines, respectively, in Figure 3B). The simulated peak had a width of 0.07 V at

half height to represent attractions among the adsorbates in addition to the potential dependence of the oxidative desorption step. The peak of the experimental voltammogram can be as high as that of the simulated voltammogram with erroneously high  $k_{\rm des}$  of 1.8 × 10<sup>4</sup> s<sup>-1</sup>. Moreover,  $k_{\rm des}$  of 4.7 × 10<sup>2</sup> s<sup>-1</sup> was determined with the non-concerted mechanism and used for the concerted mechanism to yield a much lower peak (red circles). High  $k_{\rm des}$  corresponds to high  $k_{\rm ads}$ , which is needed for the concerted mechanism to sustain the ACET step (Figure 1B).

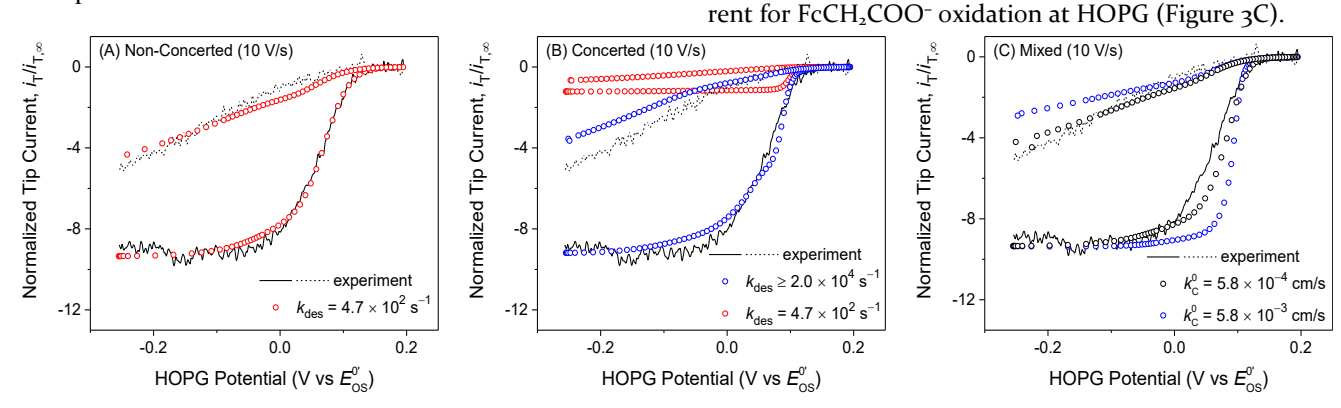


**Figure 4.** SECM measurement of Fc<sup>+</sup>CH<sub>2</sub>COO<sup>−</sup> reduction at HOPG at 10 V/s as compared with (A) non-concerted, (B) concerted, and mixed mechanisms. The identical experimental curve was obtained with 0.1 mM FcCH<sub>2</sub>COOH in 1 M KCl and 0.1 M phosphate buffer (pH = 6.2) for  $i_{T,\infty}$  = 7.1 pA during forward anodic and reverse cathodic scans of the HOPG potential (solid and dotted lines, respectively). Simulated curves (circles) were obtained with a = 333 nm, RG = 2.3, d = 30 nm in addition to (A) and (C) = 6.9 cm/s, (B) = 1.2 × 10<sup>-2</sup> cm/s, and (C) = 4.7 × 10<sup>2</sup> s<sup>-1</sup>.

We also employed slower scan rates of 0.1–5 V/s to confirm the non-concerted mechanism for both  $FcCH_2COO$ -oxidation and  $Fc^+CH_2COO^-$  reduction (Figures S-11 and S-12, respectively) at HOPG. Only the non-concerted mechanism agreed with experimental voltammograms of  $FcCH_2COO^-$  oxidation at scan rates of down to 3 V/s. The desorption step was slowed down by adsorbate–adsorbate attractions and still kinetically controlled at 3 V/s in contrast to  $FcTAM^+$  (Figure S-7B). Moreover, a good fit with experimental voltammograms at all scan rates required consistent  $k_{des}$  for the non-concerted mechanism but erroneously large  $k_{des}$  for the concerted mechanism.

We investigated the ACET reactions of ferrocenemethanol, 1,1'-ferrocenedimethanol, and tris(1,10-phenanthroline)cobalt(II) with = +3.2, $^{26} +1.2$ , $^{26}$  and -4.6, $^{44}$  respectively, to yield irreproducible SECM-based voltammograms at HOPG. The irreproducibility is attributed to the inadequate purity of the sub-millimolar

redox molecules after recrystallization. A sub-micromolar contaminant can significantly foul the HOPG surface in the solution.<sup>28</sup>

We also investigated Fc+CH2COO- reduction at HOPG

to ensure the non-concerted mechanism. The experimental voltammogram (lines in Figure 4A) fitted well

with the non-concerted mechanism with the same  $k_{\text{des}}$  of

 $4.7 \times 10^2$  s<sup>-1</sup> (red circles) as determined for FcCH<sub>2</sub>COO-oxidation (Figure 3A). The best fit required a quasi-

reversible ET step with a finite of 6.9 cm/s, which is

attributed to the self-inhibitory effect from the adsorb-

ates.44 By contrast, the experimental voltammogram devi-

ated from the voltammogram simulated for the concerted mechanism (blue circles in Figure 4B), which also re-

quired erroneously high  $k_{\rm des}$  of 1.7 × 10<sup>4</sup> s<sup>-1</sup>. The concerted

mechanism with the same  $k_{\rm des}$  of  $4.7 \times 10^2~{\rm s}^{-1}$  as the non-

concerted mechanism yielded a much lower tip current

(red circles) than observed experimentally. Moreover, the

mixed mechanism was excluded to find that must be

smaller than  $5.8 \times 10^{-4}$  cm/s to fit the experimental volt-

ammogram (Figure 4C). This analysis adjusted while

employing the same parameters as determined for the

non-concerted mechanism. The maximum of  $5.8 \times 10^{-4}$ 

cm/s also yields a good fit with the experimental tip cur-

**Implications for Electrocatalysis.** Our experimental results are used to theoretically compare ACET and outersphere ET kinetics, the competition of which determines the overall rate and product selectivity of important electrocatalytic reactions. <sup>16-19</sup> Specifically, the kinetics of adsorption-coupled and outer-sphere reduction steps are compared by considering standard free energies. The free energy change of the outer-sphere reduction step is given by where E is the electrode potential (Figure 5A). The reductive adsorption step is thermodynamically facilitated by the reductant adsorption with the standard adsorption energy, (Figure 5B). Accordingly, the free energy change of the reductive adsorption step at the more positive potential of E (Figure 5C) is equivalent to the outer-sphere counterpart at E (Figure 5A).

The of FcTMA<sup>+</sup> and FcCH<sub>2</sub>COO<sup>-</sup> (Table 1) is indicative of weak adsorption but is still comparable to the

estimated for  $O_2$  at Au(100) as a good oxygen-reduction electrocatalyst in the alkaline media. 45,46

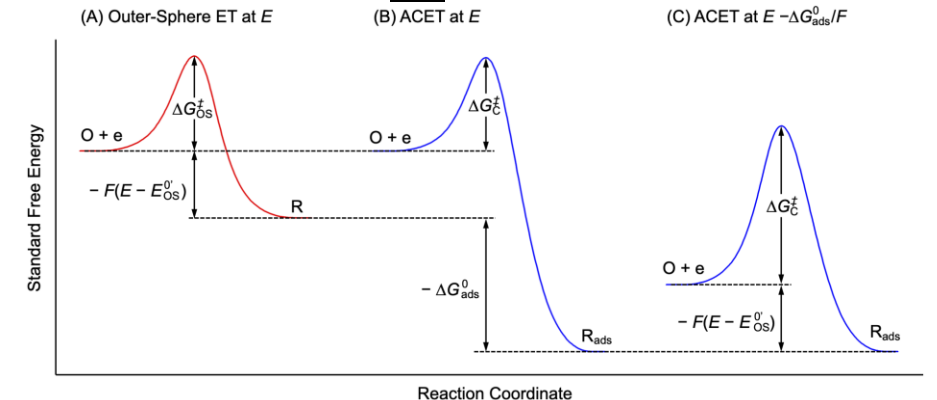


Figure 5. Standard free energy of redox-active species involved in (A) outer-sphere ET (red line) and (B) and (C) ACET (blue lines) steps.

Table 1. Comparison between  $FcTMA^+$  and  $FcCH_2COO^-$ .

adsorbate	FcTMA+	FcCH₂COO-
(eV)	-0.20 <sup>a</sup>	-0.28 <sup>b</sup>
(λ (eV)	0.26 <sup>c</sup>	0.28 <sup>c</sup>
$A_{\rm C}/A_{ m OS}$	<1.0 × 10 <sup>-4</sup>	<6.9 × 10 <sup>-4</sup>

<sup>&</sup>lt;sup>a</sup> Ref. 26. <sup>b</sup> Ref. 27. <sup>c</sup>  $\lambda$  = 0.85 eV from ref. 47.

We compare activation energies of outer-sphere and adsorption-coupled reduction steps at the same electrode potential (Figures 5A and 5B, respectively). The activation energy of the outer-sphere reduction step, is given by the Marcus theory as<sup>48</sup>

$$= \lambda/4 + \alpha_{\rm et} F(E - \square) \tag{5}$$

where  $\lambda$  is the solvent reorganization energy, and  $\alpha_{\rm et}$  (= 0.5) is the transfer coefficient. Similarly, the activation energy of the adsorption-coupled reduction step, is defined as

where is the standard activation energy of the ACET step. A comparison between eqs 5 and 6 indicates that is lower than at any potential to accelerate the adsorption-coupled reduction step in comparison with the outer-sphere counterpart when  $<\lambda/4$ .

must be lower than the outer-sphere counterpart,  $\lambda/4$ , for catalysis by the electrode.

Overall, the effect of the reductant adsorption on the adsorption-coupled reduction kinetics varies with the standard activation energy, to define Cases I, II, and III as

I.  $\lambda/4$  consists only facilitated thermodynamically

II. 
$$\lambda/4 <$$
 and  $< \lambda/4$  also accelerated

III. 
$$< \lambda/4$$
: also catalytic

For instance, is increased by the reorganization of the adsorbate-electrode interactions<sup>50</sup> as required for Cases I and II. Moreover, the dielectric constant and, subsequently, reorganization energy of water molecules can be reduced near the electrode surface,<sup>51</sup> which lowers as required for Case III.

The rates of ACET and outer-sphere ET steps depend also on the pre-exponential factor as deduced from eqs S-5 and S-7

where  $A_{\rm C}$  and  $A_{\rm OS}$  are pre-exponential factors of the respective steps. We found experimentally that was at least four orders of magnitude lower than . We assumed  $= (\lambda)/4$  as the middle value of Case II to deduce from eq 7 that  $A_{\rm C}$  can be three or four orders of magnitude lower than  $A_{\rm OS}$  (Table 1). Low  $A_{\rm C}$  is attributed to the slow dynamics of ice-like water molecules at the HOPG surface, where the ferrocene derivatives are adsorbed and solvated to participate in the ACET step. Our estimation of  $A_{\rm C}/A_{\rm OS}$  is significant because the theory for  $A_{\rm C}$  has been underdeveloped owing to the scarce availability of experimental data.

It should be noted that an ACET reaction (eq 1) may be mediated through another non-concerted mechanism

based on adsorption and inner-sphere ET steps as given respectively by<sup>2,4</sup>

$$O \blacksquare O_{ads}$$
 (8)

$$O_{ads} + e \blacksquare R_{ads}$$
 (9)

When the common adsorption step (eq 8) maintains equilibrium, inner-sphere ET and ACET steps are equivalent to each other<sup>2,4</sup> as represented by the ACET step and excluded in this work.

#### **CONCLUSIONS**

In this work, we determined the mechanism of ACET reactions experimentally for the first time. Specifically, the non-concerted mechanism of ferrocene derivatives at HOPG was identified by developing the transient voltammetric mode of nanoscale SECM. In contrast to CV,26,27 this nanoelectrochemical method kinetically controlled the adsorption step, which is required for the identification of the ACET mechanism.2,4 In addition to nonconcerted and concerted mechanisms, the mixed mechanism was considered to estimate the kinetics of the ACET step, which was not observed experimentally. These results quantitatively demonstrate that the ACET step was at least four orders of magnitude intrinsically slower than the outer-sphere ET step. The intrinsically slow ACET kinetics is attributed to the higher standard activation energy, lower pre-exponential factor, or both. These results imply that the ACET reaction is thermodynamically facilitated1 but is not necessarily accelerated or catalyzed by the reductant adsorption in comparison with the outer-sphere counterpart. We envision that SECM-based transient voltammetry will be useful as a powerful tool to resolve the coupling between the ET and specific adsorption of redox-active molecules in important electrocatalytic reactions.

#### **ASSOCIATED CONTENT**

### **Supporting Information**

The Supporting Information is available free of charge on the ACS Publications website.

Experimental details, SECM model, precise determination of desorption rate constant, thermodynamic equivalence, effect of scan rate on the FcTMA+ couple, effect of surface diffusion and tip adsorption, effect of scan rate on the FcCH₂COO-couple (PDF)

#### **AUTHOR INFORMATION**

## **Corresponding Author**

\* Shigeru Amemiya, Department of Chemistry, University of Pittsburgh, Pittsburgh, Pennsylvania 15260, United States; orcid.org/0000-0001-7357-4505; Email: amemiya@pitt.edu; Fax: 412-624-8611.

#### **ACKNOWLEDGMENT**

This work was supported by the National Science Foundation (CHE-1904258 for S.A. and DGE-1922649 for K.C.L.). N.K., D.C.J., and S.-H. H. acknowledge Arts and Sciences fellowships from the University of Pittsburgh.

#### **REFERENCES**

- (1) Bard, A. J. Inner-sphere heterogeneous electrode reactions. Electrocatalysis and photocatalysis: The challenge. *J. Am. Chem. Soc.* **2010**, *1*32, 7559–7567.
- (2) Klymenko, O. V.; Svir, I.; Amatore, C. Molecular electrochemistry and electrocatalysis: A dynamic view. *Mol. Phys.* **2014**, *112*, 1273–1283.
- (3) Bard, A. J.; Faulkner, L. R.; White, H. S. *Electrochemical methods: Fundamentals and applications*. 3rd ed.; John Wiley & Sons: New York, 2022; p 658.
- (4) Janda, D. C.; Barma, K.; Kurapati, N.; Klymenko, O. V.; Oleinick, A.; Svir, I.; Amatore, C.; Amemiya, S. Systematic assessment of adsorption-coupled electron transfer toward voltammetric discrimination between concerted and non-concerted mechanisms. *Electrochim. Acta* 2022, 428, 140912.
- (5) Seh, Z. W.; Kibsgaard, J.; Dickens, C. F.; Chorkendorff, I. B.; Norskov, J. K.; Jaramillo, T. F. Combining theory and experiment in electrocatalysis: Insights into materials design. *Science* **2017**, 355, aad4998.
- (6) Jantz, D. T.; Leonard, K. C. Characterizing electrocatalysts with scanning electrochemical microscopy. *Ind. Eng. Chem. Res.* **2018**, 57, 7431–7440.
- (7) Herrero, E.; Buller, L. J.; Abruña, H. D. Underpotential deposition at single crystal surfaces of Au, Pt, Ag and other materials. *Chem. Rev.* **2001**, *101*, 1897–1930.
- (8) Whittingham, M. S. Special editorial perspective: Beyond Li-ion battery chemistry. *Chem. Rev.* **2020**, *120*, 6328–6330.
- (9) Sluyters-Rehbach, M.; Sluyters, J. H. Some basic views on the influence of reactant adsorption on wave shapes in D.C., A.C. and linear sweep voltammetry. *J. Electroanal. Chem. Interfacial Electrochem.* 1975, 65, 831–841.
- (10) Klymenko, O. V.; Buriez, O.; Labbe, E.; Zhan, D. P.; Rondinini, S.; Tian, Z. Q.; Svir, I.; Amatore, C. Uncovering the missing link between molecular electrochemistry and electrocatalysis: Mechanism of the reduction of benzyl chloride at silver cathodes. *ChemElectroChem* **2014**, *1*, 227–240.
- (11) Atek, I.; Maye, S.; Girault, H. H.; Affoune, A. M.; Peljo, P. Semi-analytical modelling of linear scan voltammetric responses for soluble-insoluble system: The case of metal deposition. *J. Electroanal. Chem.* **2018**, *818*, 35–43.
- (12) Klymenko, O. V.; Svir, I.; Amatore, C. New theoretical insights into the competitive roles of electron transfers involving adsorbed and homogeneous phases. *J. Electroanal. Chem.* **2013**, 688, 320–327.
- (13) Chen, L.; Guo, W.; Xuan, Z.; Bi, S. Cyclic reciprocal derivative chronopotentiometric behavior of electrode process in the presence of adsorptive reactants: A theoretical study of the electrolysis sequence of adsorptive and diffusing electroactive reactants. *Electrochim. Acta* **2010**, 55, 9051–9059.
- (14) Shao, M.-H.; Liu, P.; Adzic, R. R. Superoxide anion is the intermediate in the oxygen reduction reaction on platinum electrodes. *J. Am. Chem. Soc.* **2006**, *128*, 7408–7409.
- (15) Zhang, C.; Fan, F.-R. F.; Bard, A. J. Electrochemistry of oxygen in concentrated NaOH solutions: Solubility, diffusion coefficients, and superoxide formation. *J. Am. Chem. Soc.* **2009**, 131, 177–181.

- (16) Yang, H. H.; McCreery, R. L. Elucidation of the mechanism of dioxygen reduction on metal-free carbon electrodes. *J. Electrochem. Soc.* **2000**, *147*, 3420–3428.
- (17) Ignaczak, A.; Santos, E.; Schmickler, W. Oxygen reduction reaction on gold in alkaline solutions the inner or outer sphere mechanisms in the light of recent achievements. *Curr. Opin. Electrochem.* **2019**, *14*, 180–185.
- (18) Hori, Y.; Wakebe, H.; Tsukamoto, T.; Koga, O. Electrocatalytic process of CO selectivity in electrochemical reduction of CO<sub>2</sub> at metal electrodes in aqueous media. *Electrochim. Acta* **1994**, 39, 1833–1839.
- (19) Hori, Y., Electrochemical CO<sub>2</sub> reduction on metal electrodes. In *Modern aspects of electrochemistry*, Vayenas, C. G.; White, R. E.; Gamboa-Aldeco, M. E., Eds. Springer New York: New York, NY, 2008; pp 89–189.
- (20) Chernyshova, I. V.; Somasundaran, P.; Ponnurangam, S. On the origin of the elusive first intermediate of  $CO_2$  electroreduction. *Proc. Natl. Acad. Sci. U. S. A.* **2018**, *115*, E9261–E9270.
- (21) Kai, T.; Zhou, M.; Duan, Z.; Henkelman, G. A.; Bard, A. J. Detection of CO<sub>2</sub><sup>-</sup> in the electrochemical reduction of carbon dioxide in *N*,*N*-dimethylformamide by scanning electrochemical microscopy. *J. Am. Chem. Soc.* **2017**, *139*, 18552–18557.
- (22) Kurapati, N.; Buoro, R. M.; Amemiya, S. Perspective—beyond the century-long paradigm of hydrogen electrochemistry through the Laviron–Amatore paradox. *J. Electrochem. Soc.* **2020**, *167*, 146514.
- (23) Huang, Y.-F.; Wu, D.-Y.; Wang, A.; Ren, B.; Rondinini, S.; Tian, Z.-Q.; Amatore, C. Bridging the gap between electrochemical and organometallic activation: Benzyl chloride reduction at silver cathodes. *J. Am. Chem. Soc.* **2010**, *1*32, 17199–17210.
- (24) Amemiya, S., Nanoscale scanning electrochemical microscopy. In *Electroanalytical chemistry*, Bard, A. J.; Zoski, C. G., Eds. CRC Press: 2015; pp 1–72.
- (25) Kai, T.; Zoski, C. G.; Bard, A. J. Scanning electrochemical microscopy at the nanometer level. *Chem. Commun.* **2018**, 54, 1934–1947.
- (26) Kurapati, N.; Pathirathna, P.; Chen, R.; Amemiya, S. Voltammetric measurement of adsorption isotherm for ferrocene derivatives on highly oriented pyrolytic graphite. *Anal. Chem.* **2018**, *90*, 13632–13639.
- (27) Kurapati, N.; Pathirathna, P.; Ziegler, C. J.; Amemiya, S. Adsorption and electron-transfer mechanisms of ferrocene carboxylates and sulfonates at highly oriented pyrolytic graphite. *ChemElectroChem* **2019**, *6*, 5651–5660.
- (28) Nioradze, N.; Chen, R.; Kurapati, N.; Khvataeva-Domanov, A.; Mabic, S.; Amemiya, S. Organic contamination of highly oriented pyrolytic graphite as studied by scanning electrochemical microscopy. *Anal. Chem.* **2015**, *87*, 4836–4843.
- (29) Chen, R.; Balla, R. J.; Li, Z. T.; Liu, H. T.; Amemiya, S. Origin of asymmetry of paired nanogap voltammograms based on scanning electrochemical microscopy: Contamination not adsorption. *Anal. Chem.* **2016**, *88*, 8323–8331.
- (30) Li, Z.; Kozbial, A.; Nioradze, N.; Parobek, D.; Shenoy, G. J.; Salim, M.; Amemiya, S.; Li, L.; Liu, H. Water protects graphitic surface from airborne hydrocarbon contamination. *ACS Nano* **2016**, *10*, 349–359.
- (31) Nioradze, N.; Kim, J.; Amemiya, S. Quasi-steady-state voltammetry of rapid electron transfer reactions at the macroscopic substrate of the scanning electrochemical microscope. *Anal. Chem.* **2011**, *8*3, 828–835.
- (32) Kim, J.; Izadyar, A.; Nioradze, N.; Amemiya, S. Nanoscale mechanism of molecular transport through the nuclear pore complex as studied by scanning electrochemical microscopy. *J. Am. Chem. Soc.* **2013**, *1*35, 2321–2329.

- (33) Mauzeroll, J.; Hueske, E. A.; Bard, A. J. Scanning electrochemical microscopy. 48. Hg/Pt hemispherical ultramicroelectrodes: Fabrication and characterization. *Anal. Chem.* 2003, 75, 3880–3889.
- (34) Zaino, L. P.; Wichert, W. R. A.; Crouch, G. M.; Bohn, P. W. Microchannel voltammetry in the presence of large external voltages and electric fields. *Anal. Chem.* **2016**, *88*, 4200–4204.
- (35) Nioradze, N.; Chen, R.; Kim, J.; Shen, M.; Santhosh, P.; Amemiya, S. Origins of nanoscale damage to glass-sealed platinum electrodes with submicrometer and nanometer size. *Anal. Chem.* **2013**, *85*, 6198–6202.
- (36) Kim, J.; Kim, B.-K.; Cho, S. K.; Bard, A. J. Tunneling ultramicroelectrode: Nanoelectrodes and nanoparticle collisions. *J. Am. Chem. Soc.* **2014**, *136*, 8173–8176.
- (37) Jantz, D. T.; Balla, R. J.; Huang, S.-H.; Kurapati, N.; Amemiya, S.; Leonard, K. C. Simultaneous intelligent imaging of nanoscale reactivity and topography by scanning electrochemical microscopy. *Anal. Chem.* **2021**, *93*, 8906–8914.
- (38) Barforoush, J. M.; McDonald, T. D.; Desai, T. A.; Widrig, D.; Bayer, C.; Brown, M. K.; Cummings, L. C.; Leonard, K. C. Intelligent scanning electrochemical microscopy tip and substrate control utilizing fuzzy logic. *Electrochim. Acta* 2016, 190, 713–719.
- (39) Kim, J.; Shen, M.; Nioradze, N.; Amemiya, S. Stabilizing nanometer scale tip-to-substrate gaps in scanning electrochemical microscopy using an isothermal chamber for thermal drift suppression. *Anal. Chem.* **2012**, *84*, 3489–3492.
- (40) Lefrou, C. A unified new analytical approximation for positive feedback currents with a microdisk secm tip. *J. Electroanal. Chem.* **2006**, 592, 103–112.
- (41) Pingarrón, J. M.; Labuda, J.; Barek, J.; Brett, C. M. A.; Camões, M. F.; Fojta, M.; Hibbert, D. B. Terminology of electrochemical methods of analysis (IUPAC recommendations 2019). *Pure Appl. Chem.* 2020, *92*, 641–694.
- (42) Rodriguez-Lopez, J.; Ritzert, N. L.; Mann, J. A.; Tan, C.; Dichtel, W. R.; Abruña, H. D. Quantification of the surface diffusion of tripodal binding motifs on graphene using scanning electrochemical microscopy. *J. Am. Chem. Soc.* **2012**, *134*, 6224–6236.
- (43) Amemiya, S. Comment on "impact of adsorption on scanning electrochemical microscopy voltammetry and implications for nanogap measurements": Assessment of heterogeneous self-exchange reaction at conductor and insulator. *Anal. Chem.* **2017**, *89*, 7269–7272.
- (44) Chen, R.; Najarian, A. M.; Kurapati, N.; Balla, R. J.; Oleinick, A.; Svir, I.; Amatore, C.; McCreery, R. L.; Amemiya, S. Self-inhibitory electron transfer of the Co(III)/Co(II)-complex redox couple at pristine carbon electrode. *Anal. Chem.* **2018**, *90*, 11115–11123.
- (45) Quaino, P.; Luque, N. B.; Nazmutdinov, R.; Santos, E.; Schmickler, W. Why is gold such a good catalyst for oxygen reduction in alkaline media? *Angew. Chem. Int. Ed.* **2012**, *51*, 12997–13000.
- (46) Goduljan, A.; de Campos Pinto, L. M.; Juarez, F.; Santos, E.; Schmickler, W. Oxygen reduction on Ag(100) in alkaline solutions—a theoretical study. *ChemPhysChem* **2016**, *17*, 500-505.
- (47) Chidsey, C. E. D. Free energy and temperature dependence of electron transfer at the metal-electrolyte interface. *Science* **1991**, *251*, 919–922.
- (48) Bard, A. J.; Faulkner, L. R.; White, H. S. *Electrochemical methods: Fundamentals and applications*. 3rd ed.; John Wiley & Sons: New York, 2022; p 152.
- (49) Svehla, G. Nomenclature of kinetic methods of analysis (IUPAC recommendations 1993). *Pure Appl. Chem.* **1993**, *65*, 2291–2298.

- (50) Costentin, C.; Savéant, J.-M. Catalysis of electrochemical reactions by surface-active sites: Analyzing the occurrence and significance of volcano plots by cyclic voltammetry. *ACS Catalysis* **2017**, *7*, 4876–4880.
- (51) Bangle, R. E.; Schneider, J.; Conroy, D. T.; Aramburu-Trošelj, B. M.; Meyer, G. J. Kinetic evidence that the solvent
- barrier for electron transfer is absent in the electric double layer. *J. Am. Chem. Soc.* **2020**, *142*, 14940–14946.
- (52) He, Z.-D.; Chen, Y.-X.; Santos, E.; Schmickler, W. The pre-exponential factor in electrochemistry. *Angew. Chem. Int. Ed.* **2018**, *57*, 7948–7956.

# Non-Concerted, Concerted, or Mixed?

